Transp Porous Med (2014) 101:161–189
DOI 10.1007/s11242-013-0238-7

Analytical Model for Fines Migration During Water Injection

Pavel Bedrikovetsky · Noe Caruso

Received: 5 February 2013 / Accepted: 15 October 2013 / Published online: 14 November 2013

Abstract Exact solution is derived for axisymmetric flow during water injection with fine particles detachment, migration, attachment and straining. The solution contains the so-called erosion front described as a weak discontinuity, behind which the mechanical equilibrium of attached particles holds and the dynamic attachment occurs ahead of the front. Introduction of a timely potential form for suspended concentration decreases the order of governing system allowing derivation of the erosion front trajectory. The analytical model describes the injectivity decline due to fines migration and reveals non-monotonic injection rate dependency of the well index.

Keywords Fines migration · Colloid · Porous media · Particle detachment · DLVO force · Mathematical model · Permeability decline · Injectivity

List of symbols

Variables

A_{123}	Hamaker constant ($\mathrm{ML^2T^{-2}}$)
c	Suspended particle concentration ($\mathrm{L^{-3}}$)
C	Dimensionless suspended particle concentration
D	Erosion front velocity ($\mathrm{LT^{-1}}$)
d	Collision diameter (L)
f_s	Probability density function for colloid radius
f_p	Probability density function for pore radius
F	Force ($\mathrm{MLT^{-2}}$)
h	Particle surface separation distance (L)
H	Thickness of a rectangular pore channel (L)

P. Bedrikovetsky (✉) · N. Caruso
University of Adela de, Adelaide, SA, Australia
e-mail: pavel.russia@gmail.com

J	Impedance (normalized reciprocal of well index)
k	Absolute permeability (L^2)
k_B	Boltzmann constant ($ML^2T^{-2}K^{-1}$)
l	Characteristic wavelength (L)
l_n	Normal lever (L)
l_d	Tangential lever (L)
n_∞	Bulk number density of ions (L^{-3})
p	Pressure ($MT^{-2}L^{-1}$)
P	Dimensionless pressure
PVI	Pore volume injected (dimensionless unit for time T)
q	Volumetric flow rate per unit of the reservoir production thickness (L^2T^{-1})
r	Radius (L)
r_e	Drainage radius of the well (L)
r_s	Radius of a particle (L)
S	Dimensionless retained particle concentration
t	Time (T)
$T^{/}$	Dimensionless time coordinate of intersection point of characteristics with erosion front
U	Darcy's velocity in porous media (LT^{-1})
u	Dimensionless velocity
V	Potential energy (ML^2T^{-2})
U	Dimensionless velocity
X	Dimensionless radial coordinate

Greek symbols

β	Formation damage coefficient
γ	Salinity
Δ	Difference between two values (pressure, retained concentration)
ε	Erosion number (ratio between the torques of detaching and attaching forces)
ζ	Surface potential (mV)
κ	Debye length (L^{-1})
λ	Dimensional filtration coefficient (L^{-1})
Λ	Dimensionless filtration coefficient
μ	Dynamic viscosity ($ML^{-1}T^{-1}$)
ρ	Fluid density (ML^{-3})
σ	Concentration of retained particles (L^{-3})
ϕ	Porosity
χ	Lifting force coefficient
ω	Drag force coefficient

Subscripts

cr	Critical (for attached concentration and coordinate of erosion front)
i	Initial conditions values (for suspended and retained concentrations, for erosion number)
e	electrostatic (for force)
w	Well (for radius, dimensionless radial coordinate and erosion number)

m	Maximum value (for velocity and erosion number)
n	Normal (for force)
p	Pore (for pore radius and pore size distribution)
s	Straining (for retained concentration, filtration coefficients and formation damage coefficient)
a	Attachment (for retained concentration, filtration coefficients and formation damage coefficient)
0	Initial value (for permeability and dimensionless radial coordinate)
d	Drag (for force), damage (for reservoir radius and dimensionless radial coordinate)
g	Gravitational (for force)
w	Well
BR	Born repulsion (for potential energy)
DLR	Electrostatic double layer (for potential energy)
LVA	London–van der Waal (for potential energy)

1 Introduction

Migration of natural reservoir fines occurs in many environmental, chemical and petroleum engineering processes: water production and impairment of artesian wells (Khilar and Fogler 1998; Cheng and Ouazar 2003), water injection into aquifers for fresh water storage (Cheng et al. 2003), invasion of sea water in aquifers (Bear and Cheng 1999), industrial waste disposal in subterranean reservoirs (Bradford et al. 2009, 2011, 2012), cold water injection in geothermal reservoirs (Rosenbrand et al. 2012, 2013), oil production and water injection in low consolidated, high clay content and heavy oil fields (Civan 2007). Technology development and design for the above processes are based on the results of mathematical modelling.

Usually fines migration is accompanied by severe permeability decline (Khilar and Fogler 1998; Civan 2010a,b). It is explained by lifting of the fine particles, attached to grain surfaces and pore walls by drag and lifting forces, exerting the particles from the flowing fluid. High flow velocity provides with high values of the detaching forces causing fines mobilisation. Decrease of water salinity or increase of its pH results in weakening of the attaching electrostatic force that also causes fines detachment. The lifted fines migrate in the porous space together with the carrier fluid until it meets the thinner pore throat where it is size excluded. Particle detachment leads to minor increase in permeability while the straining in thin pore throats and their plugging causes significant permeability decline.

The decline in well injectivity and productivity due to fines migration have been reported for low consolidated, high clay content and heavy oil reservoirs (Muecke 1979; Civan 2007). In the present work, an analytical model for fines migration during water injection is derived and the effects of fines migration on well injectivity are investigated.

Since the attaching and detaching forces depend on particle and pore sizes and on matrix surface mineralogy, which are stochastically distributed, numerous micro scale studies of the colloidal–suspension transport have been carried out. The population balance models account for size distributions of pores and particles (Sharma and Yortsos 1987a,b,c; Santos and Bedrikovetsky 2006). Averaging of the population balance equations results in the classical macro scale model for deep bed filtration only in the case of mono-sized suspensions (see Bedrikovetsky 2008). Multiple particle capture mechanisms can be aggregated in one mechanism with the total filtration coefficient depending on the overall retention concentration (Guedes et al. 2009). Other approaches include random walk models (Shapiro 2007;

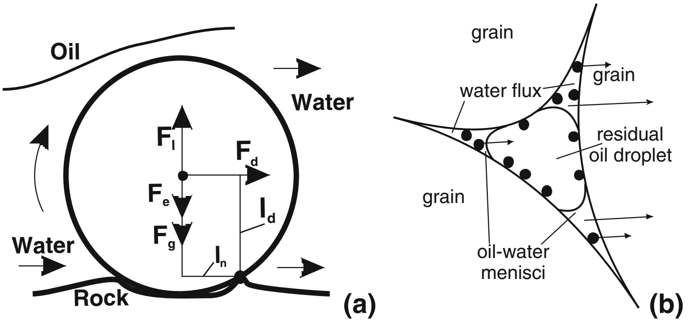

Fig. 1 Torque balance on the particle at the internal cake surface as a condition of mechanical equilibrium

Yuan and Shapiro 2010a,b), trajectory analysis (Payatakes et al. 1974; Chatterjee et al. 2011) and stochastic mean-field model (Lin et al. 2009).

The traditional model for particle detachment contains kinetic expressions for the release rates that are proportional to differences between the current and critical values of velocity, salinity, pH, stress, etc. (Ju et al. 2007; Lin et al. 2009; Bradford et al. 2009, 2012; Massoudieh and Ginn 2010). The kinetics coefficients cannot be predicted theoretically and are fully empirical parameters while the expressions for filtration coefficient are derived from micro scale models. The model exhibits the delayed response to abrupt change of velocity, salinity, pH, stress, etc., while the laboratory experiments exhibit the instant response.

Another approach to modelling of the particle detachment assumes the condition of attached particle mechanical equilibrium yielding the existence of the maximum attached concentration: the dynamic attachment occurs if the concentration of attached particles is lower than its maximum value; otherwise the mechanical equilibrium holds (Bedrikovetsky et al. 2011; Bedrikovetsky et al. 2012). The modified particle detachment model uses the maximum (critical) retention function instead of kinetics expression describing the detachment rate: if the retention concentration does not exceed its maximum value, particle capture is going on according to the classical model of deep bed filtration; otherwise, the maximum retention concentration value, which depends on flow velocity and brine ionic strength, holds. The maximum retention concentration is determined by the torque balance of electrostatic, drag, lifting and gravity forces exerting on the fine particles situated on the grain surfaces (Fig. 1a). The maximum attached concentration model is free of the above-mentioned shortcomings. Therefore, in the current paper, the modified model with maximum (critical) retention function is chosen to describe the effects of fines migration on water injection.

The axisymmetric flow with fine particles detachment, migration, attachment and straining during water injection allows for an exact solution. The distinguished feature of the solution is an erosion front—the mechanical equilibrium of attached particles holds behind the front while the attachment occurs ahead of the front. The front is a weak discontinuity, i.e. the unknown functions are continuous while their first derivatives suffer discontinuity across the wave front. Introduction of a potential form for the suspended concentration permits reducing the order of the governing system, resulting in a first-order equation for attached concentration. This equation along with the condition of mechanical equilibrium on the erosion front and the expression for attachment rate uniquely determines the trajectory of the erosion front. The analytical model reveals gradual injectivity decline with further stabilisation due to straining of the mobilised fine particles. The stabilisation time is significantly lower than a typical injection period. The fines size that affects the filtration and formation damage coefficients is the most influential parameter determining the injectivity decline due to fines migration.

The structure of the paper is as follows. Section 2 presents basic equations for fine particles lifting, straining and consequent permeability decline. The governing system for particle transport, attachment and detachment is shown in Sect. 3. Derivation of exact solution for the axisymmetric flow during water injection including implicit formulae for front trajectories and areal concentration distributions are given in Sect. 4. Section 5 presents the matching of the field data by the analytical model.

2 Fines Migration During Water Injection

In this section we briefly describe particle attachment, detachment and straining phenomena during the suspension–colloidal transport in porous media.

Fines detachment and mobilisation by drag and lifting forces, migration of released fines in porous media with the carrier water and particle straining in thin pore throats results in permeability decline and, consequently, in the well index decrease. Particle lifting occurs mainly near to wells where flow velocities and detaching forces are 2–3 orders of magnitude higher than those in the reservoir. Therefore, the most favourable region for fines detachment is the well vicinity. Since the particle straining rate is proportional to flow velocity, the intensity of size exclusion of the mobilised fines is higher near to the well. Finally, the closer to the well the permeability damaged zone is located the higher is the effect of permeability decline on well injectivity. The above are the reasons why the retention processes occur mostly in the well vicinity and why they highly affect well injectivity decline.

Particle straining is described by the linear kinetics equation where the capture rate is proportional to the advective particle flux cU (Sharma and Yortsos 1987a; Rousseau et al. 2008; Bradford et al. 2012)

$$\frac{\partial \sigma_{\mathrm{s}}}{\partial t} = \lambda_{\mathrm{s}} c U, \tag{1}$$

where U is Darcy's flow velocity, c and σ_{s} are suspended and strained particle concentrations, respectively, and λ_{s} is the filtration coefficient for straining.

Particle attachment is also described by the linear kinetics equation, but only until the maximum value of attached concentration σ_{cr} is reached (Bedrikovetsky et al. 2011)

$$\frac{\partial \sigma_{\mathrm{a}}}{\partial t} = \begin{cases} \lambda_{\mathrm{a}} c U : \sigma_{\mathrm{a}} < \sigma_{\mathrm{cr}}(\varepsilon) \\ \sigma_{\mathrm{a}} = \sigma_{\mathrm{cr}}(\varepsilon) . \end{cases} \tag{2}$$

Here σ_{a} is the attached particle concentration and λ_{a} is the filtration coefficient for attachment. The erosion number ε is the ratio between the detaching and attaching torques (see Fig. 1a where the exerting forces are shown)

$$\varepsilon = \frac{l F_{\mathrm{d}}(U) + F_{\mathrm{l}}(U)}{F_{\mathrm{e}}(\gamma) + F_{\mathrm{g}}}, \qquad l = \frac{l_{\mathrm{d}}}{l_{\mathrm{n}}} \tag{3}$$

Here F_{d}, F_{l}, F_{e} and F_{g} are drag, lifting, electrostatic and gravity forces, respectively; l_{d} and l_{n} are the lever arms for drag and normal forces. Drag and lifting forces are monotonically increasing velocity functions while electrostatic force is monotonically decreasing salinity function. So, the erosion number ε increases with velocity increase and salinity decrease. Therefore, fines mobilisation occurs with either velocity increase of salinity decrease.

The erosion number dependency of the maximum retained concentration σ_{cr} is determined from the condition of mechanical equilibrium of the fine particle on the surface of the external cake formed by the attached fines. The condition of mechanical equilibrium is the equality of detaching torques of drag and lifting forces and attaching torques of electrostatic and gravitational forces, Fig. 1. In particular, the maximum retention function as derived from the torque balance in a single cylindrical capillary is given by

$$\sigma_{\mathrm{cr}}(U)=\begin{cases}\sigma_{\mathrm{o}}\left(1-\frac{U^2}{U_{\mathrm{m}}^2}\right): U<U_{\mathrm{m}}\\ 0: \quad U\geq U_{\mathrm{m}}\end{cases} \tag{4}$$

where σ_0 is a maximum retention value corresponding to no-flow and U_{m} is a minimum velocity that drags out all attached particles from the pore surface [see Bedrikovetsky et al. (2011) for detailed derivations of Eqs. (2–4)]. Since the erosion number (3) is a velocity function, maximum retention concentration can be considered as a function of either erosion number (2) or velocity (4).

The advanced water lifts particles only from the rock surface accessible to water in water-wet rocks. The accessible area grows with the saturation increase during the displacement of oil by water (Fig. 1b). Therefore, the maximum retention function depends on water saturation; see Muecke (1979); Yuan and Shapiro (2010a,b). Well impedance depends on permeability damage in some neighbourhood of the wellbore, which is called the damaged zone; the permeability decrease outside the damaged zone does not affect the well impedance. The damaged zone size almost never exceeds 3–10 m (see Nunes et al. 2010). Fines migration occurs far behind the displacement front in damaged zone, where the residual oil saturation is already established. Therefore, during waterflooding, water saturation in damaged zone is equal to one minus residual oil saturation $1-s_{\mathrm{or}}$; permeability for water is equal to absolute permeability times relative permeability for water at the presence of residual oil k_0k_{rwor}. Initial permeability k_0 and porosity ϕ further in the text correspond to water injection into an aquifer. Injection well impedance during waterflooding can be obtained from that for single phase flow by changing permeability k_0 to k_0k_{rwor} and porosity ϕ to $\phi(1-s_{\mathrm{or}})$.

The maximum concentration dependency $\sigma_{\mathrm{cr}}(\varepsilon)$ is a phenomenological function in the model of particle detachment in porous media. This function is determined by mineralogy of rock and fines, water composition, temperature, effective stress, etc. In particular, the function depends on the pore and particle radii since its definition includes the particle radii dependencies of drag, lifting, electrostatic and gravitational forces

$$\sigma_{\mathrm{cr}}=\sigma_{\mathrm{cr}}\left[\varepsilon\left(r_{\mathrm{s}},r_{\mathrm{p}}\right)\right] \tag{5}$$

The averaged maximum retention function defined as

$$\sigma_{\mathrm{cr}}=\int\int_0^\infty \sigma_{\mathrm{cr}}\left[\varepsilon\left(r_{\mathrm{s}},r_{\mathrm{p}}\right)\right]f_{\mathrm{s}}\left(r_{\mathrm{s}}\right)f_{\mathrm{p}}\left(r_{\mathrm{p}}\right)\mathrm{d}r_{\mathrm{s}}\mathrm{d}r_{\mathrm{p}} \tag{6}$$

accounts for size distributions of pores and particles. Here f_{s} and f_{p} are particle and pore size distributions, respectively.

Figure 2 shows maximum retention function versus velocity U for different salinities. The curves have parabolic form (4). The salinity dependency of electrostatic force in (3) yields the change of maximum velocity U_{m} in (4) with salinity variation. The higher the salinity the stronger is the electrostatic particle–grain attraction and the higher is the maximum attached concentration.

The permeability increase after detachment and its decrease after straining are described by the modified Darcy's law (Sharma and Yortsos 1987a,b,c; Mays and Hunt 2005)

$$U=\frac{k_{\mathrm{o}}}{\mu\left(1+\beta_{\mathrm{a}}\sigma_{\mathrm{a}}+\beta_{\mathrm{s}}\sigma_{\mathrm{s}}\right)}\frac{\partial p}{\partial r}, \tag{7}$$

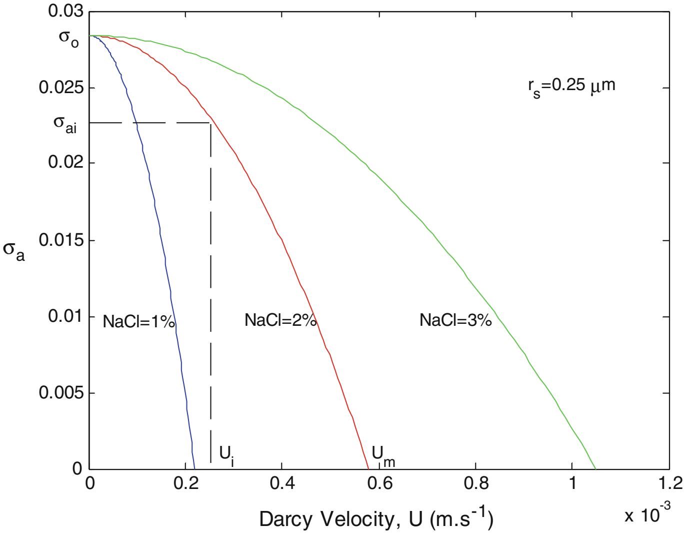

Fig. 2 Maximum retention concentration versus velocity for different brine salinities (as calculated for field case)

where the formation damage coefficient for straining usually highly exceeds that for the attachment

$$\beta_{\mathrm{a}} \ll \beta_{\mathrm{s}} \tag{8}$$

Basic relationships (1–8) for particle attachment, straining and detachment are used in the next section to form a closed system of governing equations for suspension–colloidal transport in porous media.

3 Governing Equations

Incompressibility of water and particles is assumed inside the drainage zone. The Amagat's law of volumetric additivity during particle suspension in water is also assumed.

As it follows from the flux incompressibility, the volumetric rate per unit of the reservoir production thickness q is independent of radius, i.e.

$$U(r) = \frac{q}{2\pi r} \tag{9}$$

The temperature and water composition are assumed to be constant during the injection.

Mass balance of suspended, attached and strained particles is

$$\frac{\partial}{\partial t}\left(\phi c + \sigma_{\mathrm{a}} + \sigma_{\mathrm{s}}\right) + \frac{1}{r}\frac{\partial}{\partial r}\left(\frac{cq}{2\pi}\right) = 0 \tag{10}$$

Assuming the fine particles straining in 1–10 m of well vicinity and homogeneous porous media with dispersivity 10^{-3}–10^{-2} m, the Peclet's number varies between 10^2 and 10^4. It allows neglecting the dispersive particle flux if compared with the advective flux.

Equations (1) and (2) for attachment and straining kinetics, accounting for (9), become

$$\frac{\partial \sigma_{\mathrm{a}}}{\partial t}=\begin{cases}\frac{\lambda_{\mathrm{a}} c q}{2\pi r}: \sigma_{\mathrm{a}}<\sigma_{\mathrm{cr}}(\varepsilon)\\ \sigma_{\mathrm{a}}=\sigma_{\mathrm{cr}}(\varepsilon)\end{cases} \tag{11}$$

and

$$\frac{\partial \sigma_{\mathrm{s}}}{\partial t}=\frac{\lambda_{\mathrm{s}} c q}{2\pi r} \tag{12}$$

respectively.

Modified Darcy's law, accounting for permeability decline due to attached and strained fine particles (7), becomes

$$\frac{q}{2\pi r}=\frac{k_{\mathrm{o}}}{\mu\left(1+\beta_{\mathrm{a}}\sigma_{\mathrm{a}}+\beta_{\mathrm{s}}\sigma_{\mathrm{s}}\right)}\frac{\partial p}{\partial r}. \tag{13}$$

During the straining particle capture, yielding significant permeability decline, one particle plugs one pore and vice versa. Since the particle volume is significantly lower than the pore body volume, retention concentration 10^{-3} can lead to several times decrease of permeability (Mays and Hunt 2005). Therefore, the effects of size exclusion and detachment on porosity in Eq. (10) can be neglected; further in the text, porosity ϕ is assumed to be constant.

The closed system of four governing Eqs. (10–13) determines the following unknowns: suspended, attached and strained concentrations c, σ_{a} and σ_{s}, respectively, and pore pressure p.

Introduction of dimensionless parameters—linear coordinate X, filtration coefficient Λ, time T, suspended, attached and strained concentrations C, S_{a} and S_{s}, respectively, and pore pressure P

$$X=\left(\frac{r}{r_{\mathrm{e}}}\right)^2,\quad \Lambda_k=r_{\mathrm{e}}\lambda_k,\quad T=\frac{1}{\pi\phi r_{\mathrm{e}}^2}\int_0^t q(y)\,\mathrm{d}y,\quad C=\frac{c}{\sigma_{\mathrm{ai}}},\quad S_{\mathrm{k}}=\frac{\sigma_{\mathrm{k}}}{\phi\sigma_{\mathrm{ai}}},\ k=a,s \tag{14}$$

$$P=\frac{4\pi k_{\mathrm{o}}}{q\mu}p,\quad u=\frac{2\pi r_{\mathrm{e}}U}{q} \tag{15}$$

transforms the system of Eqs. (10–13) to the dimensionless form:

$$\frac{\partial}{\partial T}\left(C+S_{\mathrm{a}}+S_{\mathrm{s}}\right)+\frac{\partial C}{\partial X}=0 \tag{16}$$

$$\frac{\partial S_{\mathrm{s}}}{\partial T}=\Lambda_{\mathrm{s}}\frac{C}{2\sqrt{X}} \tag{17}$$

$$\frac{\partial S_{\mathrm{a}}}{\partial T}=\begin{cases}\Lambda_{\mathrm{a}}\frac{C}{2\sqrt{X}}: S_{\mathrm{a}}<S_{\mathrm{cr}}(X)\\ S_{\mathrm{a}}=S_{\mathrm{cr}}(X)\end{cases} \tag{18}$$

$$1=\frac{X}{1+\phi\sigma_{\mathrm{ai}}\left(\beta_{\mathrm{a}}S_{\mathrm{a}}+\beta_{\mathrm{s}}S_{\mathrm{s}}\right)}\frac{\partial P}{\partial X} \tag{19}$$

Equations (16–18) do not contain pressure P and, therefore, can be separated from Eq. (19), i.e. pressure $P(X, T)$ is determined from Eq. (19) by substitution of the solution of the system (16–18) into Eq. (19).

As it follows from (9) and (14), the following relationship between coordinate X and dimensionless velocity u takes place

$$u = 1/\sqrt{X} \tag{20}$$

allowing redefining the maximum retention concentration from the erosion number function $\sigma_{\mathrm{cr}}(\varepsilon)$ (3, 4) and from the velocity function (4) to function of linear coordinate $S_{\mathrm{cr}} = S_{\mathrm{cr}}(X)$.

Let us determine the initial conditions for system (16–18) that correspond to the start of injection. As it follows from the assumption of the maximum retention function (2), the instant release of the excess of the initial attached concentration σ_{ai} over the function $\sigma_{\mathrm{cr}}(\varepsilon)$ occurs. Figure 2 shows that the maximum retention concentration is zero for velocities higher than the maximum velocity U_{m}, i.e. the electrostatic force cannot 'hold' the attached particles at high drag and lifting forces. Therefore, all attached particles are released in the well vicinity of $r < q/2\pi\, U_{\mathrm{m}}$. The maximum retention concentration is above the initial attached concentration for velocities lower than U_{i}, so the fines lifting in the remote area with $r > q/2\pi\, U_{\mathrm{i}}$ does not occur. Initial suspended concentration between the two zones is equal to the difference between the initial attached and maximum retention concentrations. The initial strained concentration is assumed to be zero. The above determines the initial suspended and attached concentrations:

$$C(X,0) = \begin{cases} S_{\mathrm{ai}}, & \varepsilon_{\mathrm{w}} < \varepsilon < \varepsilon_{\mathrm{m}} \\ S_{\mathrm{ai}} - S_{\mathrm{cr}}(\varepsilon), & \varepsilon_{\mathrm{m}} < \varepsilon < \varepsilon_{\mathrm{i}} \\ 0, & \varepsilon > \varepsilon_{\mathrm{i}} \end{cases} \tag{21}$$

and

$$S_{\mathrm{a}}(X,0) = \begin{cases} 0, & \varepsilon_{\mathrm{w}} < \varepsilon < \varepsilon_{\mathrm{m}} \\ S_{\mathrm{cr}}(\varepsilon), & \varepsilon_{\mathrm{m}} < \varepsilon < \varepsilon_{\mathrm{i}} \\ S_{\mathrm{ai}}, & \varepsilon > \varepsilon_{\mathrm{i}} \end{cases} \tag{22}$$

It is assumed that no strained particles are present in the rock before the injection

$$S_{\mathrm{s}}(X,0) = 0. \tag{23}$$

Particle-free water is injected; all suspended fines are those lifted during the injection; it determines the boundary condition on the well:

$$C(X_{\mathrm{w}}, T) = 0. \tag{24}$$

The exact solution of system (16–18), subject to initial-boundary conditions (21–24), is presented in the next section.

4 Analytical Model for Fines Migration During Water Injection

Exact solution of the initial-boundary value problem (21–24) for system (16–18) is formulated using the plane (X, T) (Fig. 3), where the trajectories of fronts and the characteristic lines of the solution are shown. Typical flow patterns are denoted as 0, I…XI. As the maximum retention function is velocity-dependent [see (4)] and velocity is constant along the space axis X [see (20)], the fines release occurs just once at the beginning of injection. So, there is no re-attachment of particles in zone of the initial mobilisation $X_{\mathrm{w}} < X < X_{\mathrm{i}}$. The initially released particles move ahead into zone $X > X_{\mathrm{i}}$ where there is a room for attachment, i.e. where the attached particles are 'under-saturated', $S_{\mathrm{cr}}(X) > S_{\mathrm{ai}}$. The attachment of newly arrived suspended particles occurs until the maximum retention value is reached by the

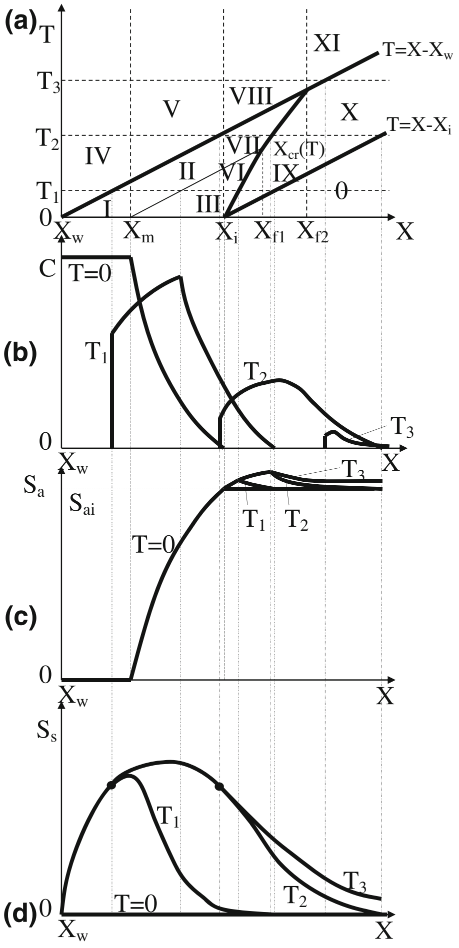

Fig. 3 Structure of the flow zone on (X, T) plane and profiles of suspended concentration, attached and strained concentrations: **a** profiles in typical moments on (X, T) plane; **b** suspended concentration profiles; **c** attached concentration profiles and **d** strained concentration profiles

attached concentration; the attachment does not occur afterwards, see Eq. (18). The above indicates that there are two different flow domains, separated from each other by an erosion front $X = X_{cr}(T)$. The erosion front is determined by the equality of attached concentration to maximum retention concentration along its trajectory $X = X_{cr}(T)$

$$S_a\left(X_{cr}\left(T\right), T\right) = S_{cr}\left(X_{cr}\left(T\right)\right). \tag{25}$$

The unknowns behind the erosion front are C and S_s while ahead of the front the unknowns are C, S_a and S_s. The solution of the system (16–18) is obtained in the following sequence. First, suspended concentration $C(X, T)$ is determined by the method of characteristics in zones I, II, III, VI, VII, IX and X assuming that the trajectory of the erosion front is known a priori. Then the attached concentration $S_a(X, T)$ in zones IX and X is determined by direct integration of rate expressions for the previously calculated suspension concentration. Provided the attachment concentration is already known, the condition (25) is a transcendental equation allowing calculating the unknown trajectory of the erosion front, $X_{cr}(T)$. Then unknown concentrations are calculated in other flow zones. Three following subsections derive the solution behind the erosion front (Sect. 4.1), determine the erosion front trajectory

(Sect. 4.2) and derive the solution ahead of the front (Sect. 4.3). Physics interpretation of the solution (Sect. 4.4) and calculations of the pressure drop using the solution (Sect. 4.5) follow.

4.1 Solution Behind the Erosion Front

Since no attachment occurs behind the erosion front (second Eq. (18) holds), the attached concentration is independent of time. Substitution of straining kinetics equation (17) into the equation for particle mass balance (16) yields

$$\frac{\partial C}{\partial T}+\frac{\partial C}{\partial X}=-\Lambda_{\mathrm{s}}\frac{C}{2\sqrt{X}}. \tag{26}$$

Equations for characteristics of the linear hyperbolic eq. (26) in zones I and II are

$$\frac{\mathrm{d}X}{\mathrm{d}T}=1,\qquad \frac{\mathrm{d}C}{\mathrm{d}T}=-\Lambda_{\mathrm{s}}\frac{C}{2\sqrt{X}}. \tag{27}$$

The characteristic velocity is equal to one, so the trajectories of characteristic lines are

$$\mathrm{X}=X_{\mathrm{o}}+T. \tag{28}$$

In terms of the initial point X_{o}, the first and second Eq. (21) provide the initial condition for the system of two ordinary differential equations (27):

$$C\left(X_{\mathrm{o}},0\right)=\begin{cases} S_{\mathrm{ai}} & X_{\mathrm{w}}<X_{\mathrm{o}}<X_{\mathrm{m}}\\ S_{\mathrm{ai}}-S_{\mathrm{cr}}\left(X_{\mathrm{o}},0\right) & X_{\mathrm{m}}<X_{\mathrm{o}}<X_{\mathrm{i}}\end{cases} \tag{29}$$

Fine particles transport in zones I, II and VII corresponds to uniform initial data [first Eq. (21)], while the non-uniform initial data [second Eq. (21)] determines the flow in zones III and VI (see Fig. 3a). The second differential eq. (27) with initial condition (29) is solved by separation of variables.

The final formulae for $C(X,T)$ in zones I, II, III, VI and VII are presented in Table 1. These formulae are valid behind the erosion front, i.e. for $X<X_{\mathrm{cr}}(T)$.

The attached concentration behind the erosion front is equal to the maximum retention function (4,5). In particular, the attached concentration is equal to zero in high velocity zones I and IV, i.e. it remains constant since the beginning of injection. It is equal to the initial attached concentration in zones II, III and V. The attached concentration profiles are built up from the rear of the erosion front and remain constant in zones VI, VII and VIII. Finally,

$$S_{\mathrm{a}}\left(X,T\right)=\begin{cases} S_{\mathrm{cr}}\left(X\right), & X_{\mathrm{m}}<X<X_{\mathrm{cr}}(T)\\ 0, & X_{\mathrm{w}}<X<X_{\mathrm{m}}.\end{cases} \tag{30}$$

The corresponding formulae for the attached concentrations in zones I, II, III, IV, V, VI, VII and VIII are presented in Table 2.

Strained concentration in zones I, II and III is determined from kinetics equation of straining rate, see Eq. (17), by integration of the suspended concentration in time T from its initial value at $T=0$, (29) to T:

$$S_{\mathrm{s}}\left(X,T\right)=\frac{\Lambda_{\mathrm{s}}}{2\sqrt{X}}\int_{0}^{T}C(X,T)\mathrm{d}T. \tag{31}$$

Since suspended concentration in zones IV, V and VIII is zero, strained concentration is steady state and is determined from its value along the injected water front $T=X-X_{\mathrm{w}}$.

Table 1 Formulae for suspension concentration in all flow domains

Zone number	Domain	Suspended concentration
0	$T < X - X_\mathrm{i}$	0
I	$X_\mathrm{w} < X < X_\mathrm{m}$ $0 < T < X - X_\mathrm{w}$	$S_\mathrm{ai}\exp\left(-\Lambda_\mathrm{s}\left(\sqrt{X}-\sqrt{X-T}\right)\right)$
II	$X_\mathrm{m} < X < X_\mathrm{i}$ $X - X_\mathrm{m} < T < X - X_\mathrm{w}$	$S_\mathrm{ai}\exp\left(-\Lambda_\mathrm{s}\left(\sqrt{X}-\sqrt{X-T}\right)\right)$
III	$X_\mathrm{m} < X < X_\mathrm{i}$ $0 < T < X - X_\mathrm{m}$	$\left(S_\mathrm{ai} - S_\mathrm{cr}\left(X-T\right)\right)\exp\left(-\Lambda_\mathrm{s}\left(\sqrt{X}-\sqrt{X-T}\right)\right)$
IV	$X_\mathrm{w} < X < X_\mathrm{m}$ $T > X - X_\mathrm{w}$	0
V	$X_\mathrm{m} < X < X_\mathrm{i}$ $T > X - X_\mathrm{w}$	0
VI	$X_\mathrm{i} < X < X_\mathrm{cr}(T)$ $T_\mathrm{cr}(X) < T < X - X_\mathrm{m}$	$\left(S_\mathrm{ai} - S_\mathrm{cr}\left(X-T\right)\right)\exp\left(-\Lambda_\mathrm{s}\left(\sqrt{X}-\sqrt{X-T}\right)\right)$
VII	$X_\mathrm{i} < X < X_\mathrm{cr}(T)$ $X - X_\mathrm{m} < T < X - X_\mathrm{w}$	$S_\mathrm{ai}\exp\left(-\Lambda_\mathrm{s}\left(\sqrt{X}-\sqrt{X-T}\right)\right)$
VIII	$X_\mathrm{i} < X < X_\mathrm{f2}$ $T > X - X_\mathrm{w}$	0
IX	$X_\mathrm{cr}(T) < X < X_\mathrm{f2}$ $X - X_\mathrm{i} < T < T_\mathrm{cr}(X)$	$C\left(X, T_\mathrm{cr}(X)\right)\exp\left(-\left(\Lambda_\mathrm{s}+\Lambda_\mathrm{a}\right)\left(\sqrt{X}-\sqrt{X_\mathrm{cr}(T)}\right)\right)$
X	$X > X_\mathrm{f2}$ $X - X_\mathrm{i} < T < X - X_\mathrm{w}$	$C\left(X, T_\mathrm{cr}(X)\right)\exp\left(-\left(\Lambda_\mathrm{s}+\Lambda_\mathrm{a}\right)\left(\sqrt{X}-\sqrt{X_\mathrm{cr}(T)}\right)\right)$
XI	$X > X_\mathrm{f2}$ $T > X - X_\mathrm{w}$	0

So, the above subsection presents the solution of the governing system (16–18) in zones I, II…VIII behind the erosion front. The trajectory of the erosion front is obtained in the next subsection.

4.2 Determining the Trajectory of the Erosion Front

The retained concentration fields $S_\mathrm{a}(X, T)$ and $S_\mathrm{s}(X, T)$ are continuous all over the (X, T) plane, while concentration $C(X, T)$ jumps across the front of the clean water injection $T = X - X_\mathrm{w}$. Yet, the concentration fields suffer discontinuities of their first derivatives along the erosion front $X = X_\mathrm{cr}(T)$ due to switching from the mechanical equilibrium of particles, given by the maximum retention function [second Eq. (2)], to non-equilibrium particle attachment [first Eq. (2)], i.e. the weak discontinuity propagates along the erosion front. Let us derive equation for the erosion front $X = X_\mathrm{cr}(T)$.

As it follows from the expressions for attachment and straining rates, i.e. from Eqs. (17) and (18), respectively,

$$C = \frac{2\sqrt{X}}{\Lambda_\mathrm{a}}\frac{\partial S_\mathrm{a}}{\partial T} = \frac{2\sqrt{X}}{\Lambda_\mathrm{s}}\frac{\partial S_\mathrm{s}}{\partial T} \tag{32}$$

the suspended concentration C becomes a timely potential for both attached and strained concentrations. From (32) it follows that

$$\frac{\partial S_\mathrm{s}}{\partial T} = \frac{\Lambda_\mathrm{s}}{\Lambda_\mathrm{a}}\frac{\partial S_\mathrm{a}}{\partial T} \tag{33}$$

Table 2 Formulae for attached concentration

Zone number	Domain	Attached concentration
0	$T < X - X_{\mathrm{i}}$	S_{ai}
I	$X_{\mathrm{w}} < X < X_{\mathrm{m}}$ $0 < T < X - X_{\mathrm{w}}$	0
II	$X_{\mathrm{m}} < X < X_{\mathrm{i}}$ $X - X_{\mathrm{m}} < T < X - X_{\mathrm{w}}$	$S_{\mathrm{cr}}(X)$
III	$X_{\mathrm{m}} < X < X_{\mathrm{i}}$ $0 < T < X - X_{\mathrm{m}}$	$S_{\mathrm{cr}}(X)$
IV	$X_{\mathrm{w}} < X < X_{\mathrm{m}}$ $T > X - X_{\mathrm{w}}$	0
V	$X_{\mathrm{m}} < X < X_{\mathrm{i}}$ $T > X - X_{\mathrm{w}}$	$S_{\mathrm{cr}}(X)$
VI	$X_{\mathrm{i}} < X < X_{\mathrm{cr}}(T)$ $T_{\mathrm{cr}}(X) < T < X - X_{\mathrm{m}}$	$S_{\mathrm{cr}}(X)$
VII	$X_{\mathrm{i}} < X < X_{\mathrm{cr}}(T)$ $X - X_{\mathrm{m}} < T < X - X_{\mathrm{w}}$	$S_{\mathrm{cr}}(X)$
VIII	$X_{\mathrm{i}} < X < X_{\mathrm{f2}}$ $T > X - X_{\mathrm{w}}$	$S_{\mathrm{cr}}(X)$
IX	$X_{\mathrm{cr}}(T) < X < X_{\mathrm{f2}}$ $X - X_{\mathrm{i}} < T < T_{\mathrm{cr}}(X)$	$S_{\mathrm{ai}} + \left(S_{\mathrm{cr}}\left(X_{\mathrm{cr}}\right) - S_{\mathrm{ai}}\right)\sqrt{\frac{X_{cr}}{X}}\exp\left(-\left(\Lambda_{\mathrm{s}} + \Lambda_{\mathrm{a}}\right)\left(\sqrt{X} - \sqrt{X_{\mathrm{cr}}}\right)\right)$
X	$X > X_{\mathrm{f2}}$ $X - X_{\mathrm{i}} < T < X - X_{\mathrm{w}}$	$S_{\mathrm{ai}} + \left(S_{\mathrm{cr}}\left(X_{\mathrm{cr}}\right) - S_{\mathrm{ai}}\right)\sqrt{\frac{X_{\mathrm{cr}}}{X}}\exp\left(-\left(\Lambda_{\mathrm{s}} + \Lambda_{\mathrm{a}}\right)\left(\sqrt{X} - \sqrt{X_{\mathrm{cr}}}\right)\right)$
XI	$X > X_{\mathrm{f2}}$ $T > X - X_{\mathrm{w}}$	$S_{\mathrm{a}}\left(X, 0\right) + \int\limits_{X-X_{\mathrm{i}}}^{X-X_{\mathrm{w}}} \frac{\Lambda_{\mathrm{a}}}{2\sqrt{X}} C_X\left(X, T\right)\partial T$

Substituting (33) into (16) yields

$$\frac{\partial}{\partial T}\left(C + S_{\mathrm{a}} + \frac{\Lambda_{\mathrm{s}}}{\Lambda_{\mathrm{a}}}S_{\mathrm{a}}\right) + \frac{\partial C}{\partial X} = 0. \tag{34}$$

Substituting first timely potential (32) into (34) and changing the order of differentiation in the second term leads to

$$\frac{\partial}{\partial T}\left[\frac{\partial}{\partial T}\left(\frac{2\sqrt{X}}{\Lambda_{\mathrm{a}}}S_{\mathrm{a}}\right) + \left(1 + \frac{\Lambda_{\mathrm{s}}}{\Lambda_{\mathrm{a}}}\right)S_{\mathrm{a}}\right] + \frac{\partial}{\partial T}\left[\frac{\partial}{\partial X}\left(\frac{2\sqrt{X}}{\Lambda_{a}}S_{\mathrm{a}}\right)\right] = 0. \tag{35}$$

Integrating both sides of (35) in T yields

$$\frac{\partial}{\partial T}\left(\frac{2\sqrt{X}}{\Lambda_{\mathrm{a}}}S_{\mathrm{a}}\right) + \left(1 + \frac{\Lambda_{\mathrm{s}}}{\Lambda_{\mathrm{a}}}\right)S_{\mathrm{a}} + \frac{\partial}{\partial X}\left(\frac{2\sqrt{X}}{\Lambda_{\mathrm{a}}}S_{\mathrm{a}}\right) = f\left(X\right), \tag{36}$$

where the time-independent function to the right hand side of (36) is determined by initial conditions (21, 22). Let us calculate the left hand side of Eq. (36) at $T = 0$ for $X > X_{\mathrm{i}}$:

$$\left.\frac{\partial S_{\mathrm{a}}}{\partial T}\right|_{T=0} = \frac{\Lambda_{\mathrm{a}}}{2\sqrt{X}}C = 0, \tag{37}$$

$$\left.\frac{\partial S_{\mathrm{a}}}{\partial X}\right|_{T=0} = \left.\frac{\partial S_{\mathrm{ai}}}{\partial X}\right|_{T=0} = 0. \tag{38}$$

Finally, the X-function in the right hand side of (36) is found from (37) and (38). Equation (36) becomes

$$\frac{\partial}{\partial T}\left(\frac{2\sqrt{X}}{\Lambda_{\mathrm{a}}}S_{\mathrm{a}}\right)+\left(1+\frac{\Lambda_{\mathrm{s}}}{\Lambda_{\mathrm{a}}}\right)S_{\mathrm{a}}+\frac{\partial}{\partial X}\left(\frac{2\sqrt{X}}{\Lambda_{\mathrm{a}}}S_{\mathrm{a}}\right)=\left(1+\frac{\Lambda_{\mathrm{s}}}{\Lambda_{\mathrm{a}}}\right)S_{\mathrm{ai}}+\frac{\partial}{\partial X}\left(\frac{2\sqrt{X}}{\Lambda_{\mathrm{a}}}S_{\mathrm{ai}}\right). \tag{39}$$

Performing differentiation on both sides of Eq. (39) yields

$$\frac{\partial S_{\mathrm{a}}}{\partial T}+\frac{\partial S_{\mathrm{a}}}{\partial X}=(S_{\mathrm{ai}}-S_{\mathrm{a}})\frac{1}{2\sqrt{X}}\left(\Lambda_{\mathrm{a}}+\Lambda_{\mathrm{s}}+\frac{1}{\sqrt{X}}\right) \tag{40}$$

Since mechanical equilibrium of fines is reached along the erosion front, the attached concentration is equal to maximum retention function along the erosion front:

$$S_{\mathrm{a}}\left(X_{\mathrm{cr}}\left(T\right), T\right)=S_{\mathrm{cr}}(X_{\mathrm{cr}}) \tag{41}$$

Taking the ordinary derivative in X of both sides of condition (41) yields

$$\frac{\mathrm{d}T_{\mathrm{cr}}}{\mathrm{d}X}\frac{\partial S_{\mathrm{a}}}{\partial T}+\frac{\partial S_{\mathrm{a}}}{\partial X}=\frac{\mathrm{d}\left(S_{\mathrm{cr}}(X)\right)}{\mathrm{d}X} \tag{42}$$

For any point $(X_{\mathrm{cr}}(T), T)$ on the erosion front, first Eq. (18), Eqs. (40) and (42) form a system of linear 3×3 equations for 3 unknowns: X- and T-derivatives of function $S_{\mathrm{a}}(X, T)$ and the erosion front velocity. Substituting first Eqs. (18) and (40) into (42) results in an explicit expression for the velocity of the erosion front

$$\frac{\mathrm{d}T_{\mathrm{cr}}}{\mathrm{d}X}=\frac{\left[\frac{\mathrm{d}(S_{\mathrm{cr}}(X))}{\mathrm{d}X}-(S_{\mathrm{ai}}-S_{\mathrm{a}})\frac{1}{2\sqrt{X}}\left(\Lambda_{\mathrm{a}}+\Lambda_{\mathrm{s}}+\frac{1}{\sqrt{X}}\right)+\frac{\Lambda_{\mathrm{a}}}{2\sqrt{X}}C\right]2\sqrt{X}}{\Lambda_{\mathrm{a}}C} \tag{43}$$

Here concentration C along the front trajectory is that obtained by the method of characteristics in zones VI and VII, see Table 1.

Let us prove that suspended concentration C is continuous along the erosion front $X_{\mathrm{cr}}=X_{\mathrm{cr}}(T)$, i.e. concentration C in Eq. (43) is that ahead or behind the front $X_{\mathrm{cr}}(T)$. Consider the condition of particle flux continuity on the front. Introduce the reference system linked to the front and moving with speed D, where D is the dislodging front speed. The relative velocity of suspended particles with respect to the reference system is $1-D$; the relative velocity of retained particles with respect to the reference system is $(-D)$.

The flux of particles behind the front is equal to that ahead of the front:

$$C^{+}\left(1-D\right)-S^{+}D=C^{-}\left(1-D\right)-S^{-}D, \tag{44}$$

where S is the total retained concentration

$$S=S_{\mathrm{a}}+S_{\mathrm{s}}. \tag{45}$$

Behind the erosion front, the retained concentration already reached its critical value

$$S^{-}=S_{\mathrm{cr}}. \tag{46}$$

As it follows from the retention rate Eqs. (17, 18), concentration $S(X, T)$ is a continuous function. In particular it is continuous across the erosion front. Therefore, $S^{+}=S_{\mathrm{cr}}$ on the erosion front, and the balance condition on the shock (44) becomes

$$\left(C^{+}-C^{-}\right)\left(1-D\right)=0 \tag{47}$$

which leaves either of two possibilities: $D = 1$ or C is continuous. Since the erosion front lags behind the characteristic that crosses point $(X_\mathrm{i}, 0)$ (Fig. 3), its velocity is less than one; the suspended concentration along the erosion front is continuous

$$C\left(X, T\right) = \begin{cases} S_\mathrm{ao}\exp\left(-\Lambda_\mathrm{s}\left(\sqrt{X_\mathrm{cr}} - \sqrt{X_\mathrm{cr} - T_\mathrm{cr}}\right)\right) \text{ for } X_\mathrm{w} < X_\mathrm{cr} - T_\mathrm{cr} < X_\mathrm{m} \\ \left(S_\mathrm{ai} - S_\mathrm{cr}\left(X_\mathrm{cr} - T_\mathrm{cr}\right)\right)\exp\left(-\Lambda_\mathrm{s}\left(\sqrt{X_\mathrm{cr}} - \sqrt{X_\mathrm{cr} - T_\mathrm{cr}}\right)\right) \text{ for } X_\mathrm{m} < X_\mathrm{cr} - T_\mathrm{cr} < X_\mathrm{i}. \end{cases} \tag{48}$$

Finally, ordinary differential eq. (43) with initial condition

$$X = X_\mathrm{i} : T = 0 \tag{49}$$

determines the trajectory of the erosion front $X = X_\mathrm{cr}(T)$.

4.3 Solution Ahead of the Erosion Front

Particle attachment occurs ahead of the erosion front, i.e. first Eq. (18) holds. Substituting it into (16) along with Eq. (17) results in

$$\frac{\partial C}{\partial T} + \frac{\partial C}{\partial X} = -\left(\Lambda_\mathrm{s} + \Lambda_\mathrm{a}\right)\frac{C}{2\sqrt{X}}. \tag{50}$$

Suspended concentration along the erosion front (48) provides boundary condition for Eq. (50). The characteristic lines with unit speed that start at the erosion front cover zones IX and X (Fig. 3a):

$$X - X_\mathrm{cr}\left(T^{/}\right) = T - T^{/} \tag{51}$$

where $T^{/}$ determines the intersection point of characteristic line (51) with erosion front and can be determined from (51) as a function of X and T by solving transcendental equation

$$T^{/} = T^{/}\left(X, T\right). \tag{52}$$

Separating variables in characteristic form of Eq. (50) yields the explicit expression for suspended concentration ahead of the erosion front in zones IX and X:

$$C\left(X, T\right) = C\left(X_\mathrm{cr}\left(T^{/}\right), T^{/}\right)\exp\left(-\left(\Lambda_\mathrm{s} + \Lambda_\mathrm{a}\right)\left(\sqrt{X} - \sqrt{X_\mathrm{cr}\left(T^{/}\right)}\right)\right). \tag{53}$$

Here the intersection point $T^{/}$ is determined from (52).

Strained concentrations along the suspension concentration front $X = X_\mathrm{i} + T$ is equal to zero. Attached concentration along the front $X = X_\mathrm{i} + T$ is equal to its initial value, i.e. S_ai. Integration of Eq. (17) in T starting from the suspension concentration front results in expressions for strained concentration

$$S_\mathrm{s}\left(X, T\right) = \int\limits_{X - X_\mathrm{i}}^{T} \frac{\Lambda_\mathrm{s}}{2\sqrt{X}} C(X, T)\mathrm{d}T. \tag{54}$$

The attached concentrations $S_\mathrm{a}(X, T)$ in zones IX and X is obtained from Eq. (40) by method of characteristics with boundary condition (41):

$$S_a(X,T) = \begin{cases} S_{ai} + (S_{cr}(X_{cr}) - S_{ai})\sqrt{\frac{X_{cr}}{X}}\exp\left(-(\Lambda_s+\Lambda_a)\left(\sqrt{X}-\sqrt{X_{cr}}\right)\right), & X_{cr} < X < T + X_i \\ S_{ai}, & X - T > X_i. \end{cases} \tag{55}$$

Formulae (53–55) are valid for zones IX and X.

Since suspended concentration in zone XI is zero, strained concentration is steady state and is determined from its value along the front $T = X - X_w$.

Formulae for suspended, attached and strained concentrations for zones 0, I, II…XI are included in Tables 1, 2 and 3. Interpretation of transport phenomena in different flow zones is presented in the next Subsection.

4.4 Structure of the Flow Zone

Figure 3a shows twelve different flow zones; formulae for concentrations in all zones are different (Tables 1, 2, 3). Figure 3b,c and d show profiles of suspended, attached and retained concentrations in three different moments, respectively.

There are two distinguished flow domains: that ahead of the erosion front where the attaching torque exceeds the detaching torque, yielding particle attaching and that behind the erosion front where the mechanical equilibrium is established and no attaching occurs.

An instant release of attached particles up to the value of maximum attached concentration occurs at the moment $T = 0$, see (21). Since velocity decreases with radius, the maximum attached concentration increases. Figure 3c shows no attached particles near to wellbore and the remaining initial attached concentration S_{ai} outside the particle mobilisation zone $X > X_i$. The released particles are mobilised into the suspension. Figure 3b shows that all detached particles near to the wellbore $X_w < X < X_m$ have been mobilised into suspension with maximum concentration. Partial release of fine particles in the intermediate zone $X_m < X < X_i$ results in the suspension profile with concentration monotonically decreasing from the maximum value at $X = X_m$ to zero at $X = X_i$. Zero suspension concentration at $X > X_i$ corresponds to no attached fines release for small velocities. The strained concentration at $T = 0$ is equal to zero (Fig. 3d).

Straight line $X = X_w + T$ is the injected water front of the injected particle-free water. Suspended concentration is zero behind this front due to piston-like dispersion-free displacement of the suspension by the clean injected water. No particles can be attached in zone $X_w < X < X_m$ at high flow velocities, so S_a remains zero in zones I and IV.

The suspended concentration profile at the moment T_1, before the erosion front catches up with the trajectory that starts at $X = X_m$, shows some increase due to decrease of retention rates (17) and (18) as X increases (Fig. 3b). Yet, the profile decreases with X in zones III and VI because the initial suspended concentration of released particles decreases with X. No suspended particles move ahead of the concentration front in zone 0 because no particles have been released there. Yet, mobilised particles move ahead of the erosion front in zones IX and X. The attached profile remains the same and equal to the maximum attached concentration in zones with $X < X_i$ since no attachment occurs behind the erosion front. Yet, some extra particles attach for $X > X_i$ due to the released particles ahead of the erosion front in zones IX and X with smaller velocities (Fig. 3c). The profile of strained concentration S_s shows an increase from zero at the wellbore due to straining of suspension with maximum suspended concentration (Fig. 3d). Further decrease of strained fines concentration with X is explained by decrease of suspended concentration and of straining rate as X increases.

Table 3 Formulae for strained concentration in different zones

Zone number	Domain	Strained concentration
0	$T < X - X_{\mathrm{i}}$	0
I	$X_{\mathrm{w}} < X < X_{\mathrm{m}}$ $0 < T < X - X_{\mathrm{w}}$	$\frac{S_{\mathrm{ai}}}{\sqrt{X}}\left[\exp\left(\Lambda_{\mathrm{s}}\left(\sqrt{X-T}-\sqrt{X}\right)\right)\left(1-\sqrt{X-T}\right)+\sqrt{X}-1\right]$
II	$X_{\mathrm{m}} < X < X_{\mathrm{i}}$ $X - X_{\mathrm{m}} < T < X - X_{\mathrm{w}}$	$\frac{S_{\mathrm{ai}}}{\sqrt{X}}\exp\left(-\Lambda_{\mathrm{s}}\sqrt{X}\right)\left[\exp\left(\Lambda_{\mathrm{s}}\left(\sqrt{X-T}\right)\right)\left(1-\sqrt{X-T}\right)\right.$ $\left.+\exp\left(\Lambda_{\mathrm{s}}\sqrt{X_{\mathrm{m}}}\right)\left(\sqrt{X_{\mathrm{m}}}-1\right)\right]+\frac{\Lambda_{\mathrm{s}}}{2\sqrt{X}}\int_{0}^{X-X_{\mathrm{m}}} C_{\mathrm{III}}(X,T)\partial T$
III	$X_{\mathrm{m}} < X < X_{\mathrm{i}}$ $0 < T < X - X_{\mathrm{m}}$	$\frac{\Lambda_{\mathrm{s}}}{2\sqrt{X}}\int_{0}^{T} C_{\mathrm{III}}(X,T)\partial T$
IV	$X_{\mathrm{w}} < X < X_{\mathrm{m}}$ $T > X - X_{\mathrm{w}}$	$\frac{S_{\mathrm{ai}}}{\sqrt{X}}\left[\exp\left(\Lambda_{\mathrm{s}}\left(\sqrt{X_{\mathrm{w}}}-\sqrt{X}\right)\right)\left(1-\sqrt{X_{\mathrm{w}}}\right)+\sqrt{X}-1\right]$
V	$X_{\mathrm{m}} < X < X_{\mathrm{i}}$ $T > X - X_{\mathrm{w}}$	$\frac{S_{\mathrm{ai}}}{\sqrt{X}}\exp\left(-\Lambda_{\mathrm{s}}\sqrt{X}\right)\left[\exp\left(\Lambda_{\mathrm{s}}\left(\sqrt{X_{\mathrm{w}}}\right)\right)\left(1-\sqrt{X_{\mathrm{w}}}\right)\right.$ $\left.+\exp\left(\Lambda_{\mathrm{s}}\sqrt{X_{\mathrm{m}}}\right)\left(\sqrt{X_{\mathrm{m}}}-1\right)\right]+\frac{\Lambda_{\mathrm{s}}}{2\sqrt{X}}\int_{0}^{X-X_{\mathrm{m}}} C_{\mathrm{III}}(X,T)\partial T$
VI	$X_{\mathrm{i}} < X < X_{\mathrm{cr}}(T)$ $T_{\mathrm{cr}}(\mathrm{X}) < T < X - X_{\mathrm{m}}$	$\frac{\Lambda_{\mathrm{s}}}{2\sqrt{X}}\left(\int_{T_{\mathrm{cr}}}^{T} C_{\mathrm{VI}}(X,T)\partial T+\int_{X-X_{\mathrm{i}}}^{T_{\mathrm{cr}}} C_{\mathrm{IX}}(X,T)\partial T\right)$
VII	$X_{\mathrm{i}} < X < X_{\mathrm{cr}}(T)$ $X - X_{\mathrm{m}} < T < X - X_{\mathrm{w}}$	$\begin{cases}\frac{\Lambda_{\mathrm{s}}}{2\sqrt{X}}\left(\begin{array}{c}\int_{T_{\mathrm{cr}}}^{X-X_{\mathrm{m}}} C_{\mathrm{VI}}(X,T)\,\partial T+\\ \int_{X-X_{\mathrm{i}}}^{T_{\mathrm{cr}}} C_{\mathrm{IX}}(X,T)\partial T+\int_{X-X_{\mathrm{m}}}^{T} C_{\mathrm{VII}}(X,T)\partial T\end{array}\right) X < X_{\mathrm{f1}}\\ \frac{\Lambda_{\mathrm{s}}}{2\sqrt{X}}\left(\int_{X-X_{\mathrm{i}}}^{T_{\mathrm{cr}}} C_{\mathrm{IX}}(X,T)\partial T+\int_{X-X_{\mathrm{m}}}^{T} C_{\mathrm{VII}}(X,T)\partial T\right) X > X_{\mathrm{f1}}\end{cases}$
VIII	$X_{\mathrm{i}} < X < X_{\mathrm{f2}}$ $T > X - X_{\mathrm{w}}$	$\begin{cases}\frac{\Lambda_{\mathrm{s}}}{2\sqrt{X}}\left(\begin{array}{c}\int_{T_{\mathrm{cr}}}^{X-X_{\mathrm{m}}} C_{\mathrm{VI}}(X,T)\,\partial T+\\ \int_{X-X_{\mathrm{i}}}^{T_{\mathrm{cr}}} C_{\mathrm{IX}}(X,T)\partial T+\int_{X-X_{\mathrm{m}}}^{X-X_{\mathrm{w}}} C_{\mathrm{VII}}(X,T)\partial T\end{array}\right) X < X_{\mathrm{f1}}\\ \frac{\Lambda_{s}}{2\sqrt{X}}\left(\int_{X-X_{\mathrm{i}}}^{T_{\mathrm{cr}}} C_{\mathrm{IX}}(X,T)\partial T+\int_{X-X_{\mathrm{m}}}^{X-X_{\mathrm{w}}} C_{\mathrm{VII}}(X,T)\partial T\right) X > X_{\mathrm{f1}}\end{cases}$
IX	$X_{\mathrm{cr}}(\mathrm{T}) < X < X_{\mathrm{f2}}$ $X - X_{\mathrm{i}} < T < T_{\mathrm{cr}}(X)$	$\frac{\Lambda_{\mathrm{s}}}{2\sqrt{X}}\int_{X-X_{\mathrm{i}}}^{T} C_{\mathrm{IX}}(X,T)\partial T$
X	$X > X_{\mathrm{f2}}$ $X - X_{\mathrm{i}} < T < X - X_{\mathrm{w}}$	$\frac{\Lambda_{\mathrm{s}}}{2\sqrt{X}}\int_{X-X_{\mathrm{i}}}^{T} C_{\mathrm{IX}}(X,T)\partial T$
XI	$X > X_{\mathrm{f2}}$ $T > X - X_{\mathrm{w}}$	$\frac{\Lambda_{\mathrm{s}}}{2\sqrt{X}}\int_{X-X_{\mathrm{i}}}^{X-X_{\mathrm{w}}} C_{\mathrm{IX}}(X,T)\partial T$

The structure of the suspension concentration wave—jump from zero on the front of injected water, increase ahead of the injected water front with further decrease down to zero on the perturbation front—remains the same in moments T_2 and T_3. Some extra attachment of released particles occurs ahead of the erosion front, the attached concentration in these zones increases with time. Straining particles accumulate in all zones with non-zero suspended concentration. The straining concentration remains constant in any point of the reservoir from the moment of passing this point by the injected water front.

Finally, the typical features of suspension transport in different flow zones are:

0 unperturbed zone without particles ahead of the concentration front;
I deep bed filtration in rock without attached particles under high velocities near the well;
II motion of the particles lifted in zone I under the presence of some attached particles;
III flow and straining of suspended fines initially lifted under the presence of remaining attached particles;
IV flow of particle-free water near the well with strained and no attached particles;
V flow of particle-free water in the rock under the presence of the attached particles remaining after the initial lifting and of the fines strained during periods II and II;
VI motion and straining of fines that arrived from zone III;
VII motion and straining of fines that arrived from zone II;
VIII flow of fines-free water in the rock under the presence of fines strained during the periods XI, VI and VII and the fines attached during the period IX;
IX suspension flow with straining and attachment in under-saturated zone behind the concentration front until the mechanical equilibrium is reached;
X suspension flow with straining and attachment in under-saturated zone behind the rear concentration front until the suspended particles are swept by the injected water;
XI fines-free water flow under the presence of the particles attached and strained during the period X.

4.5 Calculation of the Pressure Drop

Semi-analytical solution of axisymmetric flow problem derived in Sects. 4.1–4.3 allows calculating pressure drop in the drainage zone (between the well and the drainage radii, $r_{\mathrm{w}} < r < r_{\mathrm{e}}$) during the injection. The calculations are presented in the current section.

Expressing pressure gradient from Eq. (19) and integrating in X from well $X = X_{\mathrm{w}}$ to $X = 1$ yields

$$\Delta P(T) = \int_{X_{\mathrm{w}}}^{1} \frac{1 + \phi\sigma_{\mathrm{ai}}\left(\beta_{\mathrm{a}} S_{\mathrm{a}}(X,T) + \beta_{\mathrm{s}} S_{\mathrm{s}}(X,T)\right)}{X} \partial X. \tag{56}$$

The initial pressure drop across the reservoir corresponds to the absence of strained fines

$$\Delta P_{\mathrm{i}} = \int_{X_{\mathrm{w}}}^{1} \frac{1 + \beta_{\mathrm{a}}\sigma_{\mathrm{ai}}}{X} \mathrm{d}X = -\left(1 + \beta_{\mathrm{a}}\sigma_{\mathrm{ai}}\right) \ln X_{\mathrm{w}}. \tag{57}$$

Let us analyse the so-called impedance that is equal to normalised pressure drop across the reservoir during the injection

$$J(T) = \frac{\Delta P(T)}{\Delta P_{\mathrm{i}}}. \tag{58}$$

The distributions of attached and strained concentrations as taken from Tables 2 and 3 have been calculated numerically using MatLab. The impedance (58) has also been calculated by integration (56) in MatLab.

The dynamics of impedance is shown in Fig. 4 for different injection rates and water salinities. The impedance increases with time tending to some limit. The stabilisation takes

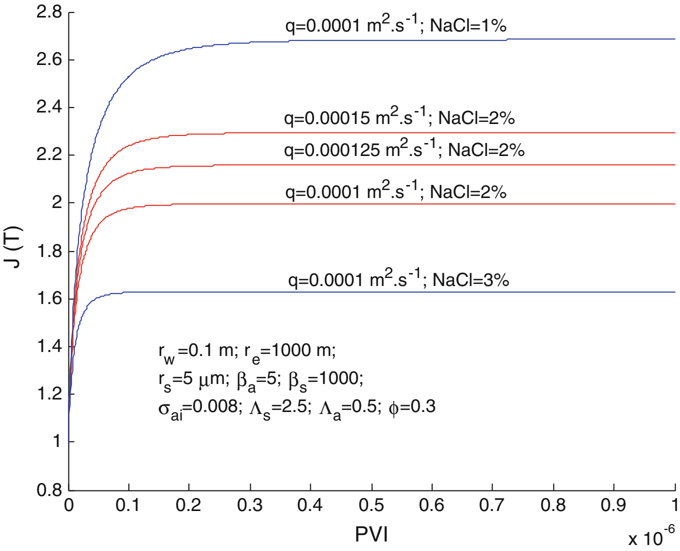

Fig. 4 Effects of injection rate and salinity on the impedance dynamics

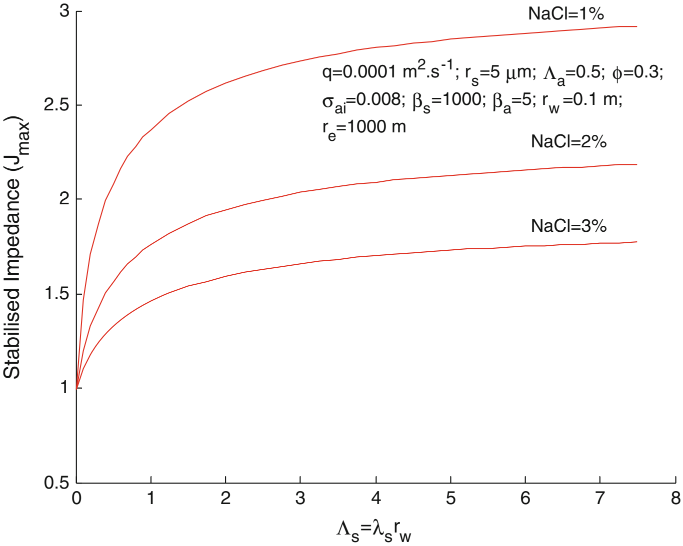

Fig. 5 Maximum impedance versus rate for different filtration coefficients/salinities

place after short-term injection remaining constant further throughout the waterflooding of the reservoir. A large number of particles are released at higher rates, so the higher the rate the higher is the impedance. The higher is the water salinity the larger is the electrostatic particle–grain attachment and the higher is the maximum attached concentration. Therefore, the higher is the salinity the smaller number of particles is released and the lower is the well impedance.

Since the impedance stabilisation occurs quickly, only its stabilised value is important for prediction of the well behaviour. Figures 5, 6 and 7 present a sensitivity study of the stabilised impedance value with respect to filtration coefficient, brine salinity and injection rate.

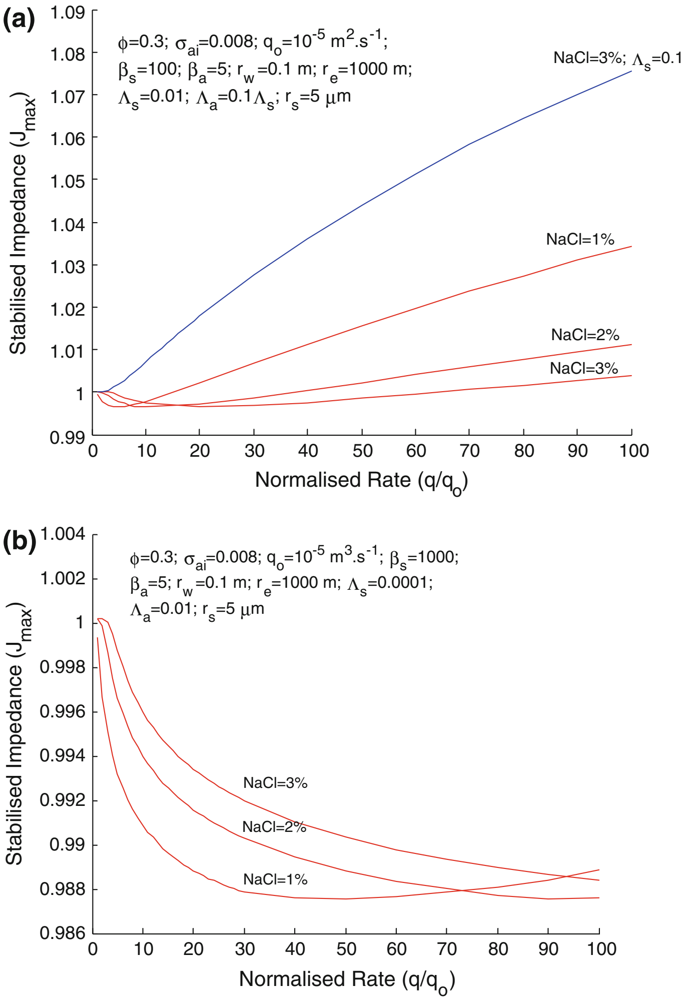

Fig. 6 Maximum impedance/skin factor versus rate for different brine salinities: **a** large fines case, **b** for small fine particles

The higher the filtration coefficient for straining the larger is the concentration of strained fines and the higher is the stabilised impedance (Fig. 5). The stabilised impedance increases with water salinity decrease due to weakening of electrostatic forces and increase in the mobilised fines concentration.

Figure 6 presents the rate dependency of the stabilised impedance. Low release and low straining occurs at low rates, so the released particles travel far away from the wellbore causing minimum damage due to straining. Injectivity increase due to particle detachment is higher than further decrease due to straining at low rates. Further rate increase causes higher increase in particle release and straining near to the wellbore yielding increase in the injectivity damage. It explains the non-monotonic rate dependency of stabilised impedance (Fig. 6a). The lower the salinity the higher is the stabilised impedance.

If fine particles are significantly smaller than pores, the straining rate is low. The rate increase causes injectivity improvement due to mobilisation of attached particles. This effect

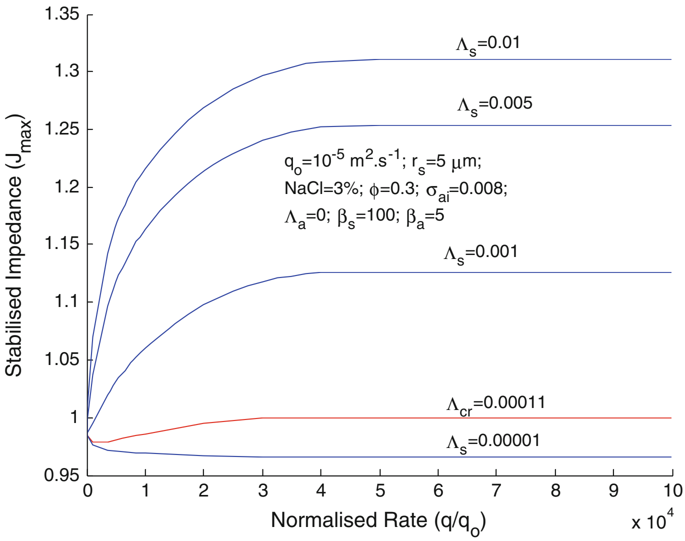

Fig. 7 Competitive permeability effects of particles release and straining: injectivity increase with the rate increase for small particles (*low curve*) and injectivity decrease with increasing rate for larger particles (*upper curves*)

is not compensated by weak straining far away from the wellbore (Fig. 6b). If fine particles are significantly smaller than pores, the straining filtration coefficient is low and the rate increase causes injectivity improvement (Fig. 7). Stabilised impedance increases for large jamming ratios.

The decision on impaired well stimulation is based on the value of the impedance that quantifies the injectivity decline. Yet, the areal spreading of the deposit is important for design of the well stimulation or damage removal technology (amount of injected acid, depth of perforation holes, etc.). So, the size of the damaged zone is another parameter revealing the extent of injectivity damage. Following Nunes et al. (2010), let us introduce the radius of the damaged zone as a minimum distance beyond which neglecting the retained concentration yields less than 5 % underestimation of well impedance. Let us consider the case where the formation damage coefficient for straining is significantly higher than that for attachment. As it follows from (56), the following equality is valid for $X = X_d$

$$\frac{\int_{X_\mathrm{w}}^{1} \frac{S_\mathrm{s}(X,T)}{X}\partial X - \int_{X_\mathrm{w}}^{X_\mathrm{d}} \frac{S_\mathrm{s}(X,T)}{X}\partial X}{\int_{X_\mathrm{w}}^{1} \frac{S_\mathrm{s}(X,T)}{X}\partial X} = 0.05. \qquad (59)$$

The damage zone size X_d is calculated from transcendental Eq. (59).

Figure 8a shows that the damaged zone size increases as the injection rate increases and the brine salinity decreases. The higher the jamming ratio the higher is the straining filtration coefficient and the fines are captured closer to the well (Fig. 8b). The effect increases as brine salinity decreases.

Figure 8 reveals that the size of damaged zone typically varies from one to ten meters. Therefore, the injectivity lost by fines migration can be restored by re-perforation only in exceptional cases where the formation damage zone size does not exceed one meter. The damaged zone size calculated by (59) can be used to determine the necessary acid volume to remove damage during well stimulation by acidizing.

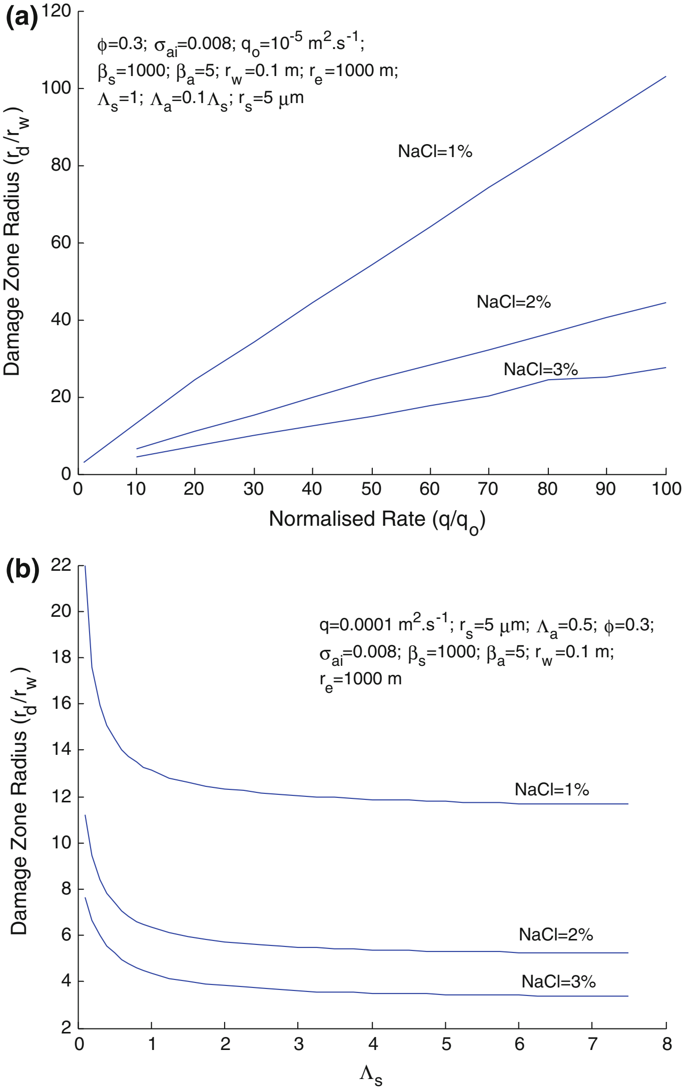

Fig. 8 Radius of the damaged zone: **a** effects of salinity and injection rate on the damaged zone size; **b** filtration coefficient and salinity dependency of the damaged size

5 Treatment of Injection Well Data

The current section presents the adjustment of field data by the analytical model.

The problem of the diagnostics of the injectivity decline mechanism is of extreme importance because it defines the technology of well damage removal, mitigation and prevention. The fines mobilisation by high rates or low salinity with migration and further straining is mentioned between the most wide spread mechanisms of well index impairment along with injection of water with solid and liquid particles, sulphate and carbonate scaling and clay swelling. Identification of the physics mechanism for injec-

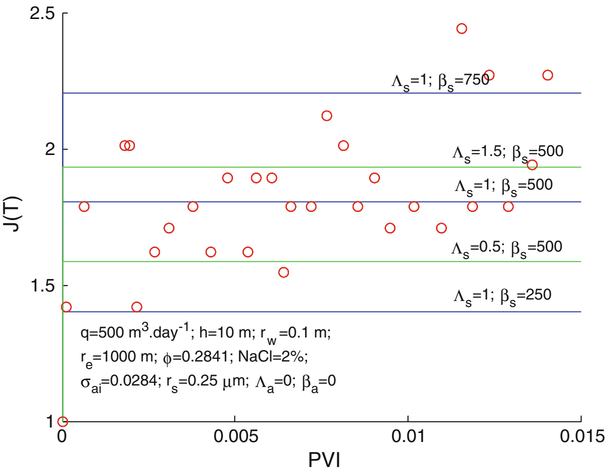

Fig. 9 Fitting of Well N1 data (field Bohai) and sensitivity with respect to filtration and formation damage coefficients

tivity decline for a concrete field case requires the extended laboratory studies and well testing.

Paper by Asghari et al. (1995) presents the field case of injectivity decline in field Siri (Iran) submitted to waterflood. Injection of water with solid particles is indicated as a physics mechanism of permeability decrease along with fines migration under high injection rates. Several laboratory tests on core injectivity and fines migration did not allow diagnosing of the permeability damage mechanism. Threefold decrease of well index occurs during 2 PVI. The lack of available data does not allow for reliable modelling accounting for both mechanisms. Nevertheless, the conclusion of instant injectivity loss at the time scale of water injection into oilfields allows dismissing fines migration as the only mechanism for injectivity decline in the Siri field.

Another case of 'competitive' mechanisms to explain injectivity decline is water injection in Bohai field (China), where fines migration and smectite swelling were nominated as possible physics mechanisms for injectivity loss (Shenglai et al. 2008). Figure 9 presents scattered data on impedance increase if compared with the initial injectivity index. The data show no timely transient from an initial impedance value $J = 1$ to average value of $J = 1.8$, i.e. a high well index decline occurs almost instantly.

Let us adjust the stabilised value of the Bohai's well impedance by the analytical model. First, we determine the electrostatic force.

Interaction between the colloidal particles (kaolinite clay particles) and the core matrix (sandstone) determines the extent of particle removal due to flow-rate alternations. Attractive long-range London–van der Waals forces and short-range electrical double-layer repulsion/attraction forces quantitatively determine such an interaction. A short-range Born repulsion force determined by the Lennard–Jones '*m*–*n*' potential takes into account the electron clouds overlapping for the case of atoms being close to each other (Elimelech et al. 1995; Habibi et al. 2012). The overall particle-surface potential energy has the following expression:

$$V = V_{\mathrm{LVA}} + V_{\mathrm{DLR}} + V_{\mathrm{BR}}, \tag{60}$$

where V_{LVA}, V_{DLR} and V_{BR} are London–van der Waals, electrostatic double-layer and Born potential energies, respectively.

The sphere–plate-retarded London–van der Waals interaction should be used in the following form according to Gregory (1981):

$$V_{\mathrm{LVA}} = -\frac{A_{123} r_{\mathrm{s}}}{6h}\left[1 - \frac{5.32h}{l}\ln\left(1 + \frac{l}{5.32h}\right)\right], \tag{61}$$

where $A_{123} = 7.73 \times 10^{-21}$ J is the Hamaker constant for a system kaolinite–water–sandstone; it is calculated according to Israelachvili (2006); the characteristic wavelength of the interaction is equal to $l = 100$ nm according to Gregory (1981); h is particle–surface separation distance, $h \ll r_{\mathrm{s}}$; r_{s} is radius of a colloidal particle.

In order to evaluate the effect of salinity variation on colloidal particle detachment, three values of NaCl were taken: 0.171, 0.342 and 0.513 M. For the above suspension salinities, three values of the product (κr_{s}) were obtained: 339, 480 and 587, respectively. In these calculations, the inverse Debye length $\kappa = 3.28 \times 10^{9} \times I^{0.5}$, m^{-1} was adopted according to Kang et al. (2004). The calculated κr_{s}-values correspond to the case where the size of the particle is significantly larger that the thickness of the double layer, according to Khilar and Fogler (1998). Gregory (1975) proposed the following formula for electrostatic double-layer potential:

$$V_{\mathrm{DLR}} = \frac{128\pi r_{\mathrm{s}} n_{\infty} k_{\mathrm{B}} T}{\kappa^{2}} \zeta_1 \zeta_2 \mathrm{e}^{-\kappa h}, \tag{62}$$

where $n_{\infty} = 6.022 \times 10^{25}$ number/m^{3} is bulk number density of ions; $k_{\mathrm{B}} = 1.381 \times 10^{23}$ J K^{-1} is the Boltzmann constant; T is the absolute temperature of the system, K; ζ_1 and ζ_2 are zeta-potentials for kaolinite and sandstone, respectively. The following zeta potential values were adopted in the present calculations: $\zeta_1 = -0.035$ mV (Stephan and Chase 2001) and $\zeta_2 = -0.026$ mV.

Born repulsion potential was evaluated according to Ruckenstein and Prieve (1976)

$$V_{\mathrm{BR}} = \frac{A_{123} d^{6}}{7560}\left[\frac{8r_{\mathrm{s}} + h}{(2r_{\mathrm{s}} + h)^{7}} + \frac{6r_{\mathrm{s}} - h}{h^{7}}\right] \tag{63}$$

where d is collision diameter, m.

Critical retention concentration was evaluated according to the model (4), where the maximum retention concentration at zero velocity assumes complete filling of the pore space by the attached particles:

$$\sigma_0\,(U = 0) = (1 - \phi_{\mathrm{c}})\,\phi \tag{64}$$

In the model (4, 64), H is the thickness of a rectangular pore channel adopted as $2r_{\mathrm{p}} = 2 \times 10^{-6}$ m; F_{e}—is the total electrostatic force calculated as the sum of attractive London–van der Waals (LvdW) and electric double-layer repulsive (DLR), and Born repulsive (BR) forces according to Derjaguin, Landau, Verwey and Overbeek (DLVO) theory (see Israelachvili 2006); $\phi_c = 0.10$ is the porosity of the cake formed on the internal surface due to colloidal particle deposition.

The following parameters are used in the present calculations: $r_{\mathrm{s}} = (0.25,\ 0.50$ and $1.0) \times 10^{-6}$ m, $T = 25\,^{\circ}\mathrm{C}$, $\rho = 1023.3$ kg m^{-3}, $r_{\mathrm{p}} = 1.0 \times 10^{-6}$ m, $\phi = 0.28$, $\omega = 5$, $\chi = 639.75$, $\mu = 1.1 \times 10^{-3}$ Pa s. Using the above model parameters, we calculated $\sigma_{\mathrm{cr}} = f(U)$-curves for various values of particle radius and salinities. Figure 2 presents maximum retention function for colloids with radius of 0.25 μ and pore size 1.0 μ.

Figure 9 presents sensitivity study of the matched stabilised impedance value with respect to filtration and formation damage coefficients. The obtained values of straining filtration and formation damage coefficients presented in Fig. 9 are the common values for these parameters.

6 Discussions

Release of particles causes some increase of permeability while their subsequent capture by size exclusion results in permeability decline, i.e. two processes are competitive. Mobilisation of particles, which are significantly smaller that pores and are not size excluded leads to injectivity increase, while the release of fine particles with size that has the same order of magnitude as the pore size results in the injectivity decline.

Let us compare the suspension flow structures given by the exact solution for axisymmetric injection (Tables 1, 2, 3) and by the solution of the linear flow problem (Bedrikovetsky et al. 2012). The flow velocity is constant during the linear flow. So, the critical retention concentration is also constant along the ‘core’. Therefore, the mobilised suspended particles are uniformly distributed after the beginning of injection; the attachment does not occur. The suspended particles perform deep bed filtration: they are carried by water and are captured by the rock with probability λ during the motion along the unit length. The suspended concentration is independent of the linear coordinate along the core and exponentially decays with time. Since the particle-free water is injected, suspended concentration is zero behind the injected water front. The strained concentration in each core point stabilises when the injected water front reaches this point.

The appearance of the erosion front moving in the reservoir away from the well is caused by non-uniform particle release during axisymmetric flow. Since the velocity decreases with radius in radial flow, the amount of released fines decreases with radius reaching zero at some distance from the well. The erosion front starts from this ‘zero’ point. The erosion front separates the forward flow domain with ‘under-saturated’ attached particles and dynamic attachment from the rear flow domain where the attached particles are in the state of mechanical equilibrium and no attachment occurs. The erosion front velocity is lower than the carrier water velocity. Therefore, the released particles bypass the erosion front and attach ahead of this front in the lower velocity zone, where the initial attached concentration is lower than the maximum retained concentration. It yields significantly more complex flow structure with radial flow rather than that during the linear flow. The attached concentration is equal to the maximum retained concentration behind the erosion front remaining ‘under-saturated’ ahead of the front. Figure 3b–d shows timely evolutions of attached, suspended and strained concentration profiles. The bank of the mobilised fines shrinks with time due to attachment ahead of the erosion front and straining in the overall flow zone. Disappearance of the suspended bank corresponds to stabilisation of attached and strained concentration profiles.

The injection rate dependency of the stabilised impedance value for small particles (low filtration coefficient) is non-monotonic due to two competitive factors of the rate increase: it causes release of more particles but they retain nearer to well. Therefore, release of small quantities of fines at low rates that retain far away from the well causes some increase of injectivity (Fig. 7a). Application of higher rates releases more particles but they are strained closer to well yielding higher injectivity damage. The effect of non-monotonic stabilised impedance versus rate increases as filtration coefficient decreases (Fig. 7b).

At high rates, where velocity exceeds the maximum speed U_{m} in well vicinity, all attached fines are mobilised. The straining rate is proportional to injection rate, so the detached particles are retained in the same vicinity. The capture becomes instant for rate tending to infinity. Therefore, the stabilised impedance becomes independent of rate at high flow rates (Fig. 8). The well injectivity increases at low filtration coefficient (small fine particles) and decreases for large fines.

The higher the injection rate the larger is the area of the released fines and the higher is the size of the damaged zone (Fig. 9a). Decrease of water salinity causes the same effect—more particles are released into moving suspension and they are captured farther. Increase of the filtration coefficient yields fines straining closer to well, resulting in damaged zone radius decrease (Fig. 9b).

The minimum well rate that would not cause the fines migration corresponds to the initial velocity of fines mobilisation U_i on the well wall, i.e. the minimum rate is equal to $2\pi\, r_\mathrm{w} U_\mathrm{i}$. Radius of the zone around the injection well where the permeability is damaged by the mobilised and strained particles has an order of magnitude of meters.

The effects of fines migration on injectivity can be important for reservoirs with low consolidated rocks and heavy oils.

As it follows from the analytical modelling data, the well impedance stabilises during fines migration almost instantly (the transient process takes around 10^{-7} PVI). On the contrary, the injectivity decline during injection of water with solid and liquid particles lasts for the periods of pore volume injection. The timely function of well index is matched by the model in the case of aqueous suspension injection, while just only the stabilised value is available for treatment by the analytical model. Therefore, a model validation from well data is significantly less informative for the case of fines mobilisation. An extensive set of field cases would allow claiming that the model for injectivity decline due to fines migration is valid. However, the extensive literature search reveals only the Bohai's well case.

The finding of the instant occurrence of the fines-induced injectivity decline can be helpful in well history analysis. Fines migration and suspension injection have been considered as possible causes for injectivity decline in field Siri. Gradual injectivity decrease allows concluding that fines migration cannot be the only cause.

The present work discusses constant rate injection. The axisymmetric problem (21–24) allows for exact solution for the case of piecewise constant rate. The solution allows investigating how high initial rate may 'clean up' the injection well.

The derived formula for strained fines concentration exhibits monotonic permeability growth k(r) from well into the reservoir. The formulae may be used in the interpretation of well test data for radius-dependent permeability (Feitosa et al. 1994; Thompson and Reynolds 1997).

7 Conclusions

Fines lifting near to injection wells due to high drag and lifting forces, further fines migration and straining are described by the analytical model consisting of the transcendental equations. The lifting of the natural reservoir fines occurs near injector from the beginning of injection almost instantly. The mobilised fines migrate and form the erosion front; the fines partly attach to the rock surface ahead of the front while the steady-state profile of attached particles is formed behind the front. The attachment torque exceeds the detaching torque ahead of the erosion front while the mechanical equilibrium is established behind the front.

High rate injection causes the injectivity decline for large values of filtration coefficient, i.e. for large fine particles and for strong 'particle-grain' attraction. For low filtration coefficients (small fines, weak ‘particle-grain’ attraction or repulsion) the high rate injection results in some injectivity enhancement.

The effects of fines mobilisation on well injectivity increase with the injection rate increase.

The lower the salinity, the weaker are electrostatic attracting forces, the higher is the mobilised fines concentration and the higher is the injectivity decline. This effect is stronger for high filtration coefficients.

The higher the filtration coefficient, the higher is the fraction of the mobilised particles that retains in the rock and the higher is the stabilised impedance value.

For the case of small particles and, consequently low filtration coefficient, the injection rate dependency of stabilised impedance can be non-monotonic.

The stabilised impedance value is independent of injection rate for high values of injection rate.

Skin factor induced by fines migration and straining monotonically increases with time and then stabilises. According to laboratory-based modelling, the injectivity decreases 2–3 times until stabilisation, and the typical values of the typical stabilisation time have order of magnitude 10^{-7} PVI, that corresponds to several hours for high rate wells and few days for low rate wells. Therefore, the injectivity decline due to fines migration occurs instantly at the reservoir exploitation time scale.

The values of the model parameters (filtration and formation damage coefficients, maximum retention concentration) that match the injectivity decline case in Bohai offshore field are in the range of common intervals. However, more field cases must be analysed for validation of the model developed.

The formula for formation damage zone size can be used for planning and design of the injection well stimulation by acidizing, re-perforation or other damage removal and mitigation technology.

Acknowledgments The authors are grateful to Dr A Badalyan (The University of Adelaide) for assistance in modelling of the electrostatic interactions. Dr Zhenjiang You (The University of Adelaide) is gratefully acknowledged for fruitful discussions and for help in preparing the manuscript. The study is generously sponsored by the Australian Research Council and Santos Ltd.

References

Ahfir, N.D., Benamar, A., Alem, A., Wang, H.Q.: Influence of internal structure and medium length on transport and deposition of suspended particles: a laboratory study. J. Transp. Porous Media **76**, 289–307 (2009)

Asghari, K., Kharrat, R., Vassouhi, S.: Alteration of permeability by fine particle movement—a water injectivity problem. In: SPE International Symposium on Oilfield Chemistry, San Antonio, TX, USA, 14–17 February 1995

Bear, J., Cheng, A.H.-D.: An overview. In: Bear, J., Cheng, A.H.-D., Sorek, S., Ouazar, D., Herrera, I. (eds.) Seawater Intrusion in Coastal Aquifers—Concepts, Methods, and Practices, pp. 1–8. Kluwer, Dordrecht (1999)

Bedrikovetsky, P.G.: Upscaling of stochastic micro model for suspension transport in porous media. J. Transp. Porous Media **75**(3), 335–369 (2008)

Bedrikovetsky, P., Siqueira, F.D., Furtado, C., de Souza, A.L.S.: Modified particle detachment model for colloidal transport in porous media. J. Transp. Porous Media **86**, 353–383 (2011)

Bedrikovetsky, P., Zeinijahromi, A., Siqueira, F.D., Furtado, C., de Souza, A.L.S.: Particle detachment under velocity alternation during suspension transport in porous media. J. Transp. Porous Media **91**(1), 173–197 (2012)

Bradford, S., Kim, H., Haznedaroglu, B., Torkzaban, S., Walker, S.: Coupled factors influencing concentration-dependent colloid transport and retention in saturated porous media. J. Environ. Sci. Technol. **43**, 6996–7002 (2009)

Bradford, S., Torkzaban, S., Simunek, J.: Modeling colloid transport and retention in saturated porous media under unfavorable attachment conditions. Water Resour. Res. **47**(10), W1050-3–W1050-11 (2011)

Bradford, S., Torkzaban, S., Morales, V., Zhang, W., Harvey, R., Packman, A., Mohanram, A., Welty, C.: Transport and fate of microbial pathogens in agricultural settings. Crit. Rev. Environ. Sci. Technol. (2012). doi:10.1080/10643389.2012.710449

Cheng, A.H.-D., Ouazar, D.: Coastal Aquifer Management-Monitoring, Modeling, and Case Studies. Lewis Publishers, London (2003)

Cheng, A.H.-D., Benhachmi, M.K., Halhal, D., Ouazar, D., Naji, A., EL Harrouni, K.: Pumping optimization in saltwater-intruded aquifers. In: Cheng, A.H.-D., Ouazar, D. (eds.) Coastal Aquifer Management—Monitoring, Modeling, and Case Studies, pp. 233–256. Lewis Publishers, London (2003)

Civan, F.: Reservoir Formation Damage (Fundamentals, Modeling, Assessment, and Mitigation), 2nd edn. Gulf Professional Publishing, Oxford (2007)

Civan, F.: Temperature effect on power for particle detachment from pore wall described by an Arrhenius-type equation. J. Trans. Porous Media **67**, 329–334 (2010a)

Civan, F.: Non-isothermal permeability impairment by fines migration and deposition in porous media including dispersive transport. J. Transp. Porous Media **85**(1), 233–258 (2010b)

Chatterjee, R., Mitra, S., Bhattacharjee, S.: Particle deposition onto janus and patchy spherical collectors. Langmuir **27**, 8787–8797 (2011)

Elimelech, M., John, G., Xiadong, J., Richard, W.: Particle Deposition and Aggregation: Measurement, Modelling, and Simulation. Butterworth-Heinemann, New York (1995)

Feitosa, G.S., Lifu, C., Thompson, L.G., Reynolds, A.C.: Determination of permeability distribution from well-test pressure data. J. Petroleum Technol. **47**, 607–615 (1994)

Gregory, J.: Interaction of unequal double layers at constant charge. J. Colloid Interface Sci. **51**(1), 44–51 (1975)

Gregory, J.: Approximate expressions for retarded van der waals interaction. J. Colloid Interface Sci. **83**(1), 138–145 (1981)

Guedes, R.G., Al-Abduwani, F., Bedrikovetsky, P., Currie, P.: Injectivity decline under multiple particle capture mechanisms. Soc. Petroleum Eng. J. **8**, 477–487 (2009)

Habibi, A., Ahmadi, M., Pourafshary, P., Al-Wahaibi, Y.: Reduction of fines migration by nanofluids injection: an experimental study. Soc. Petroleum Eng. J. **27**(14), 1–10 (2012)

Israelachvili, J.: Intermolecular and Surface Forces. Academic Press, London (2006)

Ju, B., Fan, T., Wang, X., Qui, X.: A new simulation framework for predicting the onset and effects of fines mobilization. J. Transp. Porous Media. **68**, 265–283 (2007)

Khilar, K., Fogler, S.: Migration of Fines in Porous Media. Kluwer Academic Publishers, Dordrecht (1998)

Kang, S., Subramani, A., Hoek, E.M.V., Deshusses, M.A., Matsumoto, M.R.: Direct observation of biofouling in cross-flow microfiltration: mechanisms of deposition and release. J. Membr. Sci. **244**, 151–165 (2004)

Lin, K., Pryadko, L., Walker, S., Zandi, R.: Attachment and detachment rate distributions in deep-bed filtration. Phys. Rev. E. **79**, 046321-1–046321-12 (2009)

Mays, D., Hunt, J.: Hydrodynamic aspects of particle clogging in porous media. J. Environ. Sci. Technol. **39**(2), 577–584 (2005)

Massoudieh, A., Ginn, T.R.: Colloid-facilitated contaminant transport in unsaturated porous media, Chapter 8. In: Hanrahan, G. (ed.) Modelling of Pollutants in Complex Environmental Systems, vol. II. ILM Publications, Glensdale (2010)

Muecke, T.W.: Formation fines and factors controlling their movement in porous media. J. Petroleum Technol. **31**(2), 144–150 (1979)

Nunes, M., Bedrikovetsky, P., Newbery, B., Furtado, C.A., Souza, A.L.: Theoretical definition of formation damage zone with applications to well stimulation. J. Energy Res. Technol. **132**, 33101-1–33101-7 (2010)

Payatakes, A.S., Rajagopalan, R., Tien, C.: Application of porous medium models to the study of deep bed filtration. Can. J. Chem. Eng. **52**(6), 722–731 (1974)

Rousseau, D., Hadi, L., Nabzar, L.: Injectivity decline from produced water re-injection: new insight on in-depth particle-deposition mechanisms. Soc. Petroleum Eng. J. **23**(4), 525–531 (2008)

Ruckenstein, D.C., Prieve, D.C.: Adsorption and desorption of particles and their chromatographic separation. AIChE J. **22**, 276 (1976)

Rosenbrand, E., Fabricius, I., Yuan, H.: Thermally induced permeability reduction due to particle migration in sandstones: the effect of temperature on kaolinite mobilisation and aggregation. In: Proceedings of 37th Workshop on Geothermal Reservoir Engineering Stanford University, Stanford, California, January 30–February 1 (2012)

Rosenbrand, E., Fabricius, I., Kets, F.: Kaolinite mobilisation in sandstone: pore plugging vs suspended particles, pp. 11–13. In: Proceedings of 38th Workshop on Geothermal Reservoir Engineering Stanford University, Stanford, California, February (2013)

Santos, A., Bedrikovetsky, P.G.: A Stochastic model for particulate suspension flow in Porous Media. J. Transp. Porous Media **13**, 30–52 (2006)

Shapiro, A.A.: Elliptic equation for random walks. Application to transport in micro-porous media. Physica A **375**(1), 81–96 (2007)

Shapiro, A.A., Wesselingh, J.A.: Gas transport in tight porous media. Gas Kinet. Approach. Chem. Eng. J. **142**, 14–22 (2008)

Sharma, M.M., Kuo, J.F., Yen, T.F.: Further investigation of the surface charge properties of oxide surfaces in oil-bearing sands and sandstones. J. Colloid Interface Sci. **115**(1), 9–16 (1987)

Sharma, M.M., Yortsos, Y.C.: Transport of particulate suspensions in porous media: model formulation. AIChE J. **33**(13), 1636–1643 (1987a)

Sharma, M.M., Yortsos, Y.C.: A network model for deep bed filtration processes. AIChE J. **33**(13), 1644–1653 (1987b)

Sharma, M.M., Yortsos, Y.C.: Fines migration in porous media. AIChE J. **33**(13), 1654–1662 (1987c)

Shenglai, Y., Zhichao, S., Wenhui, L., Zhixue, S., Ming, W., Jianwei, Z.: Evaluation and prevention of formation damage in offshore sandstone reservoirs in China. Petroleum Sci. **5**(4), 340–347 (2008)

Stephan, E.A., Chase, G.G.: A preliminary examination of zeta potential in deep bed filtration activity. Sep. Purif. Technol. **21**(3), 219–226 (2001)

Thompson, L.G., Reynolds, A.C.: Well testing for radially heterogeneous reservoirs under single and and multiphase flow conditions. Soc. Petroleum Eng. J. SPEFE **12**(1), 57–64 (1997)

Wang, J., Liu, H., Wang, Z., How, P.: Experimental investigation on the filtering flow law of pre-gelled particle in porous media. J. Transp. Porous Media **94**, 69–86 (2012)

Wong, R., Mettananda, D.: Permeability reduction in Qishn Sandstone specimens due to particle suspension injection. J. Transp. Porous Media **81**, 105–122 (2010)

Yortsos, Y.C., Shankar, K.: Asymptotic analysis of pore-closure reactions. Ind. Eng. Chem. Fundam. **23**, 132–134 (1984)

Yuan, H., Shapiro, A.A.: A mathematical model for non-monotonic deposition profiles in deep bed filtration systems. Chem. Eng. J. **166**(1), 105–115 (2010a)

Yuan, H., Shapiro, A.A.: Modeling non-Fickian transport and hyperexponential deposition for deep bed filtration. Chem. Eng. J. **162**, 974–988 (2010b)